

Lifetime of quasi-particles in the nearly-free electron metal sodium

D.V. Potorochin,^{1,2,3} R. Kurlito,^{4,5} O.J. Clark,⁶ E.D.L. Rienks,⁶ J. Sánchez-Barriga,⁶
F. Roth,^{1,7} V. Voroshnin,⁶ A. Fedorov,⁴ W. Eberhardt,⁸ B. Büchner,^{4,9} and J. Fink^{4,9,*}

¹*Institute of Experimental Physics, TU Bergakademie Freiberg, Leipziger Straße 23, 09599 Freiberg, Germany*

²*European XFEL, Holzkoppel 4, 22869 Schenefeld, Germany*

³*Deutsches Elektronen-Synchrotron DESY, Notkestrasse 85, 22607 Hamburg, Germany*

⁴*Leibniz Institute for Solid State and Materials Research Dresden, Helmholtzstr. 20, 01069 Dresden, Germany*

⁵*Department of Physics, University of Colorado, Boulder, CO, 80309, USA*

⁶*Helmholtz-Zentrum Berlin, Albert-Einstein-Strasse 15, 12489 Berlin, Germany*

⁷*Center for Efficient High Temperature Processes and Materials Conversion (ZeHS),
TU Bergakademie Freiberg, 09599 Freiberg, Germany*

⁸*Center for Free-Electron Laser Science/DESY, 22607 Hamburg, Germany*

⁹*Institut für Festkörperphysik, Technische Universität Dresden, 01062 Dresden, Germany*

(Dated: August 19, 2022)

We report a high-resolution angle-resolved photoemission (ARPES) study of the prototypical nearly-free-electron metal sodium. The observed mass enhancement is slightly smaller than that derived in previous studies. The new results on the lifetime broadening increase the demand for theories beyond the random phase approximation. Our results do not support the proposed strong enhancement of the scattering rates of the charge carriers due to a coupling to spin fluctuations. Moreover, a comparison with earlier electron energy-loss data on sodium yields a strong reduction of the mass enhancement of dipolar electron-hole excitations compared to that of monopole hole excitations, measured by ARPES.

I. INTRODUCTION

The understanding of electron-electron ($e-e$) many-body interactions in metals is an ongoing challenge in solid-state physics since many decades. These interactions are of great interest because they determine transport, thermal, and magnetic properties of metals. There are also many indications, that $e-e$ interaction, e.g. spin fluctuations [1] mediates unconventional superconductivity in cuprates and ferropnictides. These interactions are the subject of numerous experimental and theoretical studies during the last decades. Very often, they start from the classical behavior of normal metals (Fermi liquids) assuming that these are well understood.

Here we report a study of the simplest nearly-free-electron metal Na. Even in this prototypical Fermi liquid metal, there are unresolved issues. Numerous attempts have been made to understand the electronic structure including the mass enhancement $m^*/m = 1.28$, using integrated and angle-resolved photoemission spectroscopy (ARPES) [2–7]. The mass renormalization is related to the real part of the self-energy $\Re\Sigma$. Various state-of-the-art many-body techniques were used, starting with the random phase approximation (RPA) [8], theories beyond RPA including the GW formalism with all types of approximations (GW+) [9–14]. Correlation effects have been discussed in Refs. [15–17]. There are ongoing discussions about the influence of spin fluctuations [18]. More recently, a strong increase of the scattering rate Γ due to a strong coupling to spin fluctuations was pre-

dicted, but not a corresponding increase of the mass enhancement [19]. Γ is related to the inverse lifetime τ and to the imaginary part of the self-energy by the relation $\Gamma = -2Z\Im\Sigma$, where Z is the renormalization function, which for a less correlated material is expected to be constant and close to the Fermi level equal to $Z=m/m^*$ [20].

The early ARPES studies on the mass enhancement of the quasi-particles in Na [5–7] were performed with an energy resolution of 0.3 eV. No linewidth analysis has been performed in these studies. Here we report not only on the mass enhancement, but also on the energy dependence of the lifetime broadening with an energy resolution, which is improved by a factor of 10 compared to the earlier experiments. To the best of our knowledge, no data on the lifetime broadening of photoholes in Na have been published in the literature.

Based on our new ARPES data we hope that we contribute to the general understanding of many-body problems in normal metals (Fermi liquids), which may also help to understand the normal state of cuprate superconductors (marginal Fermi liquids [21]), and iron pnictides which show “super Planckian scattering rates” [22–24].

II. EXPERIMENTAL

The experiments were performed at the 1² ARPES endstation using the UE 112-PGM-2a beamline. Additional experiments were performed at the Spin-ARPES end station of the U125-2-PGM beamline. As a substrate we used a W(110) single crystal. This crystal was cleaned before deposition by annealing in O atmosphere (1×10^{-7} mbar) at 1200 °C followed by flashing at 2200 °C. The quality of the W(110) surface was verified by LEED ex-

* Corresponding author. E-mail address: J.Fink@ifw-dresden.de.

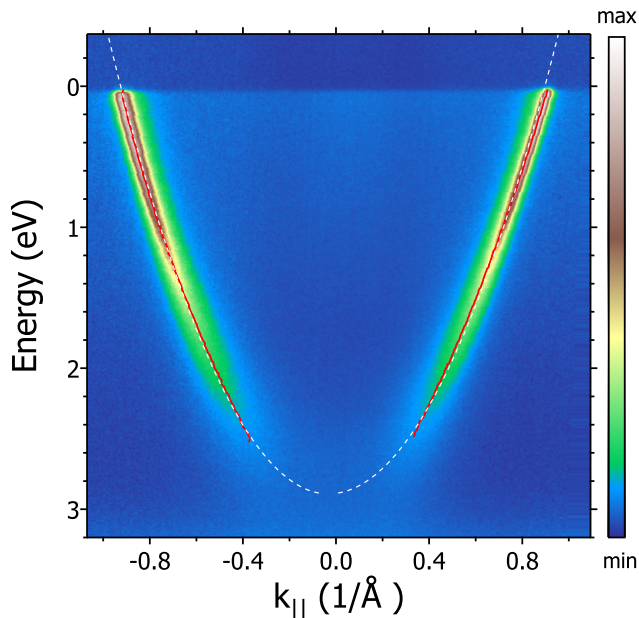


FIG. 1. Experimental energy-momentum distribution map of Na measured along the k_y direction using horizontally polarized photons. Red line: dispersion derived from a Lorentzian fit to momentum distribution curves. White dashed line: fit of the maxima of the Lorentzians with a parabolic dispersion.

periments, core level spectroscopy on the W $4f$ level, and by ARPES experiments.

Na was evaporated out of a Mo crucible on the single crystalline W substrate, cooled to 20 K. Subsequently, the sample was annealed for 15 minutes at room temperature. Most of the results reported here were obtained from a Na(110) film having a thickness of about 15 nm. During measurements, the temperature of the crystal was 20 K. The base pressure of the experimental setup was better than $6 \cdot 10^{-11}$ mbar. Photoelectrons were detected with a Scienta R8000 electron analyzer. The overall experimental energy and momentum resolutions were set to 30 meV and 0.2° , respectively.

III. III. EXPERIMENTAL RESULTS

In Fig. 1 we show an energy-momentum distribution map measured with a photon energy of $h\nu = 70$ eV along $k_{\parallel} = k_y = \Gamma - N = \langle 100 \rangle$ at a k_z value corresponding to the Γ point in the third Brillouin zone (BZ). The Γ point has been determined from similar photon-energy-dependent spectra described in Appendix A. We determined the dispersion $E(k)$ by fitting momentum distribution curves (MDC) with Lorentzians. The white dashed line is a fit of the derived dispersion with a parabola.

The spectral weight at the bottom of the band is rather low when compared with that at the Fermi level. The reason for this is related to matrix element effects. The initial state has predominantly s character, i.e., it

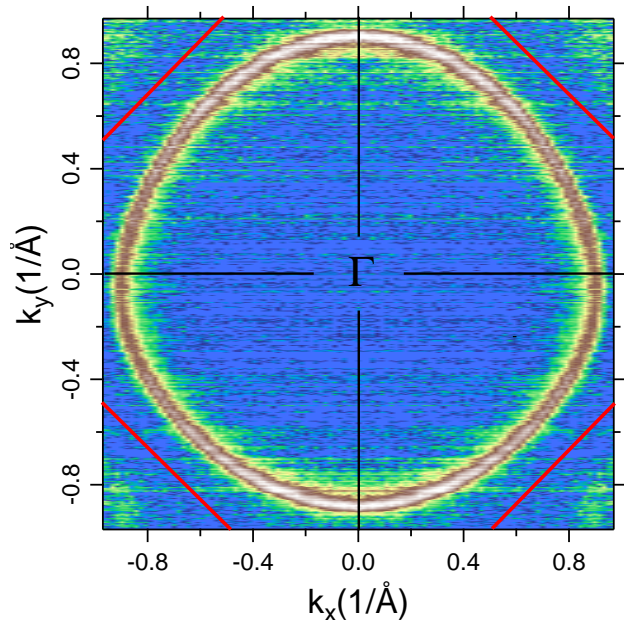


FIG. 2. Experimental Fermi surface map of Na(110) measured with horizontally ($\parallel k_x$) polarized photons. The data are symmetrized relative to $k_x = 0$. Red lines: part of the Brillouin zone.

is even with respect to the $k_x - k_z$ mirror plane. We measured with photons having a horizontal polarization. This means the dipole operator is even relative to that mirror plane. The vanishing intensity could indicate that the final states, which according to dipole excitation must be of p -character, are predominantly odd with respect to the scattering plane. The situation is very similar to our previous study of the waterfall dispersion of the spectral weight in Nd_2CuO_4 [25].

In Fig. 2 we depict the Fermi surface of Na(110) measured with a photon energy of $h\nu = 70$ eV in the $k_z = \Gamma, k_x - k_y$ plane. The data were derived by a summation of intensities in an energy range of 0.015 eV close to the Fermi level. The Fermi surface is close to a circle as expected for a nearly-free-electron metal. The Fermi wave vector along the k_y line is $k_F = 0.91$ $1/\text{\AA}$. The small deviations from a circular Fermi surface detected in the present experiment are caused possibly by a flattening and splitting of the dispersion due to the proximity to the Brillouin zone (BZ), or by a non-perfect angle calibration of the lens parameters or alignment.

In the corners of Fig. 2 we detect a faint signal of the Fermi surface of the second BZ. This observation indicates that the orientation of the Na(110) single crystal is along the main high symmetry lines. This also supports that the momentum distribution map, presented in Fig. 1, is measured along the $\langle 100 \rangle$ (k_y) direction.

In Fig. 3 we present a waterfall plot of momentum distribution curves as a function of energy together with an “all at once fit” [26]. For the fit we use a quartic dispersion $E(k) = W - \gamma_1 k^2 - \gamma_2 k^4$. A small deviation from a

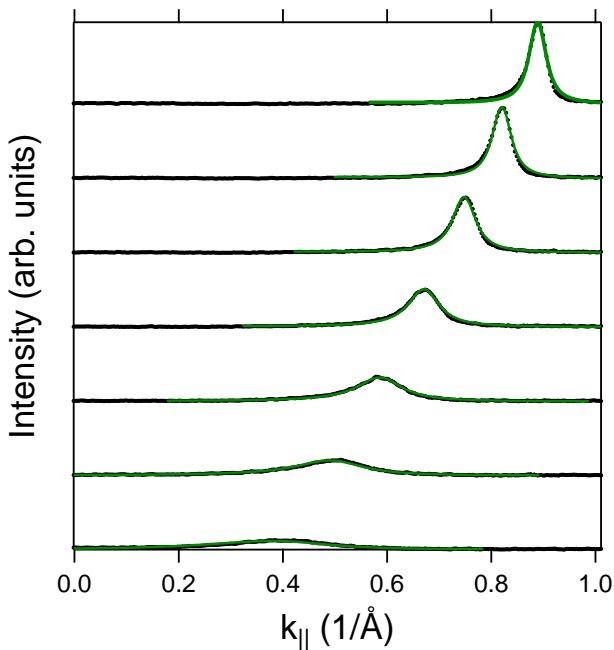


FIG. 3. Waterfall plot of ARPES momentum distribution curves of the valence band as a function of energy (black dots) in the energy range $0.103 \leq E \leq 2.263$ eV, measured along k_y (see Fig. 1 and 2). Green line: “all-at-once” fits of the spectral function with energy dependent lifetime broadening and including corrections from finite energy and momentum resolution.

free-electron parabolic dispersion was also derived from band structure calculations for Na [27]. From the fit we obtain the following parameters: $W = 2.78$ eV, $\gamma_1 = 3.77$ eVÅ², $\gamma_2 = -0.49$ eVÅ⁴, and the total line width broadening $\Gamma(E)_{\text{exp}}$, corrected for finite experimental resolution, for each energy. From a comparison of the bottom of the band W with that derived from LDA band structure calculations ($W_{\text{LDA}} = 3.18$ eV [27]), a mass renormalization $m^*/m_0 = 1.14$ is calculated.

We emphasize, that we do not use the traditional method for the evaluation of the energy dependence of the line width, i.e., fitting the momentum distribution curves with Lorentzians and multiplication the derived widths in momentum space with the velocity. Rather we fit the two-dimensional data with the spectral function described with parameters related to the width in energy space at each energy.

To obtain the lifetime broadening of the photohole $\Gamma_h^{\text{in}}(E)$ due to $e-e$ interaction, we have to subtract contributions from elastic scattering $\Gamma_h^{\text{el}}(E)$ and/or a broadening due to a finite inverse lifetime Γ_e of the photoelectrons.

First, we assume that the finite value $\Gamma_h^{\text{el}}(0)$ is completely determined by impurity scatterers. The constant mean distance d between the impurities is equal to $1/\Delta k$, where Δk is the momentum width at the Fermi level. Then the broadening due to elastic scattering is given by $v(E)\Delta k$, where $v(E)$ is the energy-dependent group

velocity taken from the experiments.

Second, we assume that the broadening at k_F is caused by the finite lifetime broadening Γ_e of the final-state photoelectron, which is usually termed “final state effect”. For normal emission, the final state broadening leads at the Fermi level to a broadening $(v_h(E)/v_e(E))\Gamma_e$ [28–36], where $v_h(e)$ and $v_e(E)$ are the photohole and photoelectron group velocities, respectively. Then the inelastic scattering rate of the photoholes is given by $\Gamma_h^{\text{in}}(E) = \Gamma_{\text{exp}}(E) - (v_h/v_e)\Gamma_e$. For the more general corrections in the off-normal case, we use the register-line formalism [37–39] which is discussed in detail in Appendix B. We conclude that in the analyzed energy range we get a very similar inelastic scattering rate $\Gamma_h^{\text{in}}(E)$ regardless of whether we apply corrections caused by elastic scattering or by “final state effect”. Using the mean value of such corrections we obtain the inverse hole lifetime $\Gamma_h^{\text{in}}(E)$ which is depicted in Fig. 4. The result can be fitted using the relation $\Gamma(E) = \alpha E^n$ with $\alpha = 0.131 \pm 0.012$ and $n = 1.98 \pm 0.08$ (see Fig. 4). In Appendix B we depict the uncorrected curve which, at the Fermi level has a finite value of 0.18 eV.

The real and the imaginary part of the self-energy are connected by the Kramers-Kronig transformation (KKT). This means that an enhancement of the scattering rate leads in tandem to an enhancement of the effective mass. Using the renormalization constant $Z = m/m^* = 0.88$ from the band width renormalization we have calculated $\Im\Sigma(E) = -\Gamma(E)/2Z$. Upon performing the KKT of $\Im\Sigma(E)$ we obtain $\Re\Sigma(E)$. From this, the mass renormalization $m^*/m = 1 + \Re\Sigma(E)/E = 1.18$ can be calculated. This value is close to the value obtained directly from the band renormalization (see above and Table I).

IV. DISCUSSION

The dispersion, derived from the data in Fig. 1 is very close to a parabola. This is expected for a nearly-free-electron metal. A possible kink due to electron-phonon coupling would appear at very low energies because of the low Debye energy $\Theta_D = 0.013$ eV of Na [40] and it would be very weak because the electron-phonon coupling should be small in a nearly-free-electron system such as the non-superconducting Na. In Table I we compare the band width and the mass enhancement (assuming a parabolic dispersion) with results from the Plummer group and theoretical calculations. The reduction of the band width when compared with that from LDA calculations [27] is slightly less than that of the early ARPES study. Correspondingly, also the mass enhancement is slightly smaller. On the other hand, the deviations compared to the earlier values are not very pronounced. This means that the discussion of the band width reduction should follow earlier work. The free-electron RPA calculations yield mass enhancements which are too small and the GW approximation or local

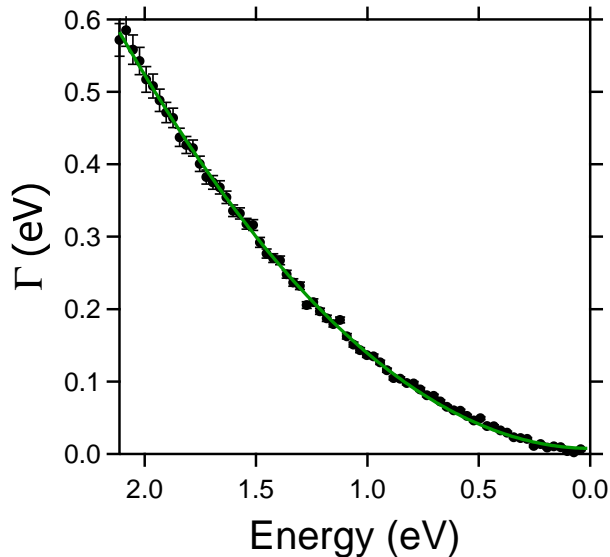


FIG. 4. Inelastic (e-e) scattering rates Γ of photoholes in Na as a function of energy. Black dots: corrected ARPES data derived from the fit presented in Fig. 3. Green solid line: fit with $\Gamma_h^{\text{in}}(E) = \alpha E^n$.

field corrections are needed to describe the experimental data (see Table I).

The energy dependence of the line width is almost perfectly quadratic. The exponent $n = 1.98 \pm 0.08$ is very close to two. The quadratic energy dependence extends over a large energy range up to 2.2 eV corresponding to a temperature of 25000 K.

The prefactor α is considerably higher than that of the RPA free-electron value of Quinn and Ferrel ($\alpha = 0.076$) [8]. Because the real part of the self-energy, determining the band width, and the imaginary part, determining the lifetime, is connected via the KKT, this difference is expected when regarding the data in Table I. Thus, our data on the lifetime broadening demand that one has to go *beyond* RPA. This is expected because Na with an r_S value close to 4 is not a high-density Fermi liquid. Theoretical calculations using the GW approximation or local field corrections are closer to the experimental data. On the other hand, the calculations by Lischner *et al.* [19] postulating the importance of spin fluctuations for the scattering rate yield a much too high pre-factor α (see Table I). Thus our experimental results do not support the proposed strong coupling of the conduction electrons to spin fluctuations in Na.

Comparing the α value of the valence electrons in Na with $\alpha = 0.24$ derived for surface states in the 4d metal Mo [41] signals the expected enhanced scattering rate in 4d metals relative to that of sp metals.

Next we discuss a comparison of our ARPES data with data of interband and intraband excitations in Na [44] measured by EELS. From the cutoff of interband transitions a mass enhancement $m^*/m = 1.05 \pm 0.04$ was derived. A similar value $m^*/m = 1.0$ was obtained from

TABLE I. ARPES data of Na compared with theoretical data from the literature: ARPES, present work; ARPES/KKT effective mass derived by a Kramers-Kronig transformation of the scattering rate; ARPES from Plummer's group; RPA FEG, free-electron gas; RPA LDA; GW LDA + plus approximations; GW LDA SF plus spin fluctuations. W : band width, m^*/m mass renormalization using $W_{\text{LDA}} = 3.18$ eV from LDA calculations [27]. α : pre-factor from the fit of the corrected scattering rates. Γ_e : lifetime broadening of the photoelectron

	W (eV)	m^*/m	α (1/eV)	Γ_e (eV)
ARPES ^a	2.78	1.14	0.131 ± 0.012	$\lesssim 4.8$
ARPES/KKT ^b		1.18		
ARPES ^c	2.5-2.61	1.28		
RPA FEG ^d	2.96	1.10	0.05-0.077	3.3
RPA LDA ^e			0.1	3.3
GW + ^f	2.52-2.89	1.11-1.26	0.10-0.34	
GW LDA SF ^g	2.51	1.27	0.47	

^a ARPES, present work

^b ARPES+KKT, present work

^c Refs. [5-7]

^d Refs. [8, 9, 11, 20, 42, 43]

^e Ref. [11]

^f Refs. [12, 19]

^g Ref. [19]

the analysis of zone boundary collective states (ZBCS), a combination of intraband and interband excitations from the band bottom to states near the BZ. The inconsistency between the ARPES and the EELS data on the effective mass was already previously noticed [45]. It can be rationalized in the following way: EELS measures inter- or intraband excitations, i.e., two particle or electron-hole excitations with dipole character. They are less screened than single-hole or monopole excitations detected in ARPES experiments.

Final state effects may have far-reaching implications for the interpretation of all ARPES data. E. g., in Ref. [46] it is claimed, that the mass renormalization of the valence electrons detected in ARPES is related to final state effects. This interpretation can be ruled out because a similar mass enhancement $m^*/m = 1.256$ has been detected in de-Haas-van-Alphen effect measurements [47].

Assuming that the momentum width $\Delta k_F = 0.045$ 1/Å is predominantly caused by elastic scattering we derive a mean-free path of the photoelectrons at the Fermi level of $1/\Delta k_F = 22$ Å.

Assuming that the broadening at the Fermi level is predominantly caused by the finite lifetime of the photoelectrons, we derive the result $\Gamma_e = 4.8$ eV. This value is in rather good agreement with the value of about 3 eV estimated for 100 eV electrons in Na from an analysis of LEED data [28] or the theoretical value calculated on the basis of a coupling to plasmons in a free-electron model (RPA) [20] or using RPA LDA [11] predicting $\Gamma_e = 3.3$ eV. Using a free-electron approximation one can also estimate the mean-free path of 70 eV photoelectrons in Na: $v_e/\Gamma_e = 6$ Å. This value is close to 8 Å resulting from core

level photoelectron experiments [36]. The agreement of our results for the lifetime broadening and the mean-free path of the photoelectrons with those in the literature supports our evaluation of the lifetime of the photohole as a function of energy.

V. SUMMARY

In the present high-resolution ARPES study of the prototypical nearly-free electron metal sodium, we confirm previous results of the mass enhancement of the charge carriers, although with a slightly smaller value. In addition, we present the energy dependence of the lifetime broadening. A perfect quadratic energy dependence is observed. The prefactor is enhanced compared to RPA calculations. The reason is that sodium is not in the high-density region, thus expecting slightly larger scattering rates caused by many-body interactions. The central result of our sodium ARPES study is, that it does not support the theoretical prediction of a rather strong enhancement of the lifetime broadening of the quasi-particles due to a coupling to spin fluctuations. A comparison with excitations studied with EELS indicates, that those dipolar two-particle excitations are much less screened than the single-particle excitations studied by ARPES.

VI. ACKNOWLEDGMENTS

J. S.-B. gratefully acknowledges financial support from the Impuls- und Vernetzungsfonds der Helmholtz-Gemeinschaft.

Appendix A: 3D NATURE OF THE FERMI SURFACE

In addition to the k_{\parallel} dependence of the Fermi wave vector presented in the main paper, we have also performed photon energy dependent ARPES experiments to obtain information on the k_z dependence of the Fermi surface. ARPES data of the Fermi wave vector k_F as a function of the wave vector k_z are presented in Fig. 5. We have added a scale of the photon energy. The experimental data were fitted by

$$k_F(k_z) = (\bar{k}_F^2 - (k_z - k_{z0})^2)^{0.5}. \quad (\text{A1})$$

We obtain for the average Fermi wave vector $\bar{k}_F = 0.88$ ($1/\text{\AA}$), which is close to the value $k_F = 0.91$ ($1/\text{\AA}$) derived from the $k_{\parallel} = k_y$ dependent dispersion presented in the main paper. The maximum of $k_F(k_z)$ appears at $k_z = 4.48$ ($1/\text{\AA}$) or $h\nu = 69$ eV. This shows that the photon energy $h\nu = 70$ eV used in the main paper is close to a value corresponding to a plane with $k_z = 0$. The results demonstrate the nearly-free 3D nature of the Fermi surface.

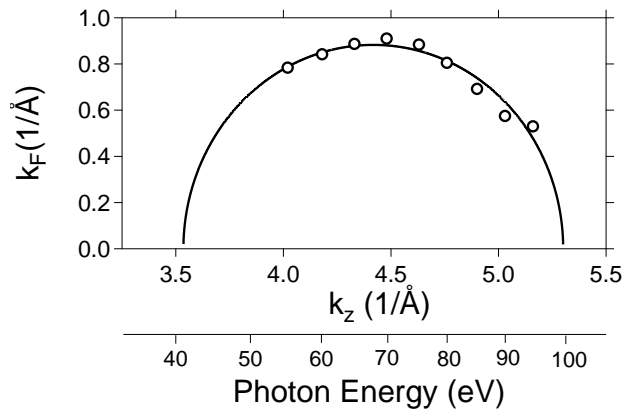


FIG. 5. Fermi wave vector k_F (black markers) of sodium as a function of the photoelectron wave vector k_z , normal to the sample surface, or the photon energy. Black solid line: least square fit of the data to a circular Fermi surface.

Appendix B: CORRECTIONS FOR ELASTIC SCATTERING AND FINAL STATE EFFECTS

The experimental data on scattering rates Γ_{exp} are composed out of three contributions: the inelastic scattering rate of the photohole Γ_h^{in} , which is the central quantity of the main paper, the elastic scattering rate of the photohole Γ_h^{el} due to impurities, and contributions due to the finite lifetime broadening of the excited photoelectron in the final state Γ_e . In a Fermi liquid, at the Fermi surface, Γ_h^{i} is expected to be zero. Then $\Gamma_{\text{exp}}(0)$ is the sum of $\Gamma_h^{\text{el}}(0)$ and $\Gamma_e(0)$. If the energy dependence of the latter two quantities is known, the experimental scattering rates can be corrected in the entire energy range to yield $\Gamma_h^{\text{i}}(E)$ [2, 28–36, 39].

In Fig. 6 we plot the total lifetime broadening derived from the ARPES data shown in Fig. 3 of the main paper. As described above, the finite offset at the Fermi level is due to the elastic scattering $\Gamma_h^{\text{el}}(0)$ and/or due to $\Gamma_e(0)$.

First, we discuss the case where the offset is completely determined by elastic scattering. Usually, it is assumed that the elastic scattering rate Γ_h^{el} is independent of the energy E . As it is caused by elastic scattering by impurities which are separated by a mean distance d , the inverse lifetime $1/\tau^{\text{el}} = \Gamma_h^{\text{el}} = dv_h$, where v_h is the group velocity of the quasiparticles/photoholes. Close to the Fermi level, it is a good approximation to assume a linear dispersion from which follows that v_h is constant and therefore Γ_h^{el} should be constant. On the other hand, in the present work, we study the spectral weight over a large energy range and the dispersion is parabolic leading to an energy dependent velocity. Close to the Fermi level it is high while at the bottom of the band it is zero. Thus, the elastic scattering rate should be $\Gamma_h^{\text{el}}(E) = (v_h(E)/v_h(0))\Gamma_h^{\text{el}}(0)$. The corrected values $\Gamma_h^{\text{in}}(E) = \Gamma_{\text{exp}}(E) - \Gamma_h^{\text{el}}(E)$ are presented

in Fig. 6 by green markers. From a least squares fit with $\Gamma_h^{\text{in}} = \alpha E^n$, we obtain the parameters $\alpha = 0.118 \pm 0.002$ and $n = 2.06 \pm 0.02$.

Next, we discuss the case where the offset of the width at the Fermi level is completely determined by a finite lifetime broadening of the photoelectrons. Following the register-line formalism [37–39], the experimental broadening Γ_{exp} is given by

$$\Gamma_{\text{exp}} = (\Gamma_h + R\Gamma_e)/(1 - R). \quad (\text{B1})$$

where Γ_h and Γ_e are the inverse lifetime of the photohole and the photoelectron, respectively. R is given by

$$R = \frac{\hat{e} \cdot \nabla_{\mathbf{k}} E_h}{\hat{e} \cdot \nabla_{\mathbf{k}} E_e}. \quad (\text{B2})$$

\hat{e} is a unit vector which is tangential to the RL, and \hat{y} and \hat{z} are unit vectors determining the $y - z$ scattering plane.

We approximate the dispersion of the photohole and the photoelectron by a free-electron band $E = (\hbar^2/2m)(k_y^2 + k_z^2)$. Then the gradients in Eq. B2 are

$$\nabla_{\mathbf{k}} E(k) = (\hbar^2/m)(\hat{y}k_y + \hat{z}k_z). \quad (\text{B3})$$

For a free photoelectron state the RL is given by

$$k_z = \left(\frac{2m_0}{\hbar^2} V_0 + k_y^2 \cot^2 \Theta \right)^{\frac{1}{2}}. \quad (\text{B4})$$

Θ is the scattering angle relative to \hat{z} . The inner potential $V_0 = 10$ eV was derived from the energy dependent ARPES experiment on Na [5]. It is consistent with our data presented in Fig. 5 of Appendix A. The unit vector \hat{e} is determined by

$$\hat{e} = \hat{y}e_y + \hat{z}e_z = \frac{\hat{y} + \hat{z}(k_y/k_z) \cot^2 \Theta}{((k_y/k_z)^2 \cot^4 \Theta + 1)^{\frac{1}{2}}} \quad (\text{B5})$$

In the present experiment, we measure the photohole dispersion for $k_z = 0$. Then combining Eqs. B3 and B5 and using a renormalized free-electron band with an effective mass m^* , we obtain

$$R = \sin^2 \Theta / m^* \quad (\text{B6})$$

For a Fermi liquid the photohole broadening $\Gamma_h(0)$ at the Fermi level is zero and assuming that the elastic scattering broadening is negligible, the experimental broadening $\Gamma_{\text{exp}}(E)$ is completely caused by the lifetime broadening of the photoelectron, which can be calculated from

$$\Gamma_e = \Gamma_{\text{exp}}(0)(1 - R(0))/R(0). \quad (\text{B7})$$

On the other hand, if the final state broadening Γ_e is known, the photohole broadening Γ_h can be derived from the experimental data Γ_{exp} . This has been discussed and demonstrated in numerous papers in the literature [28–36, 39].

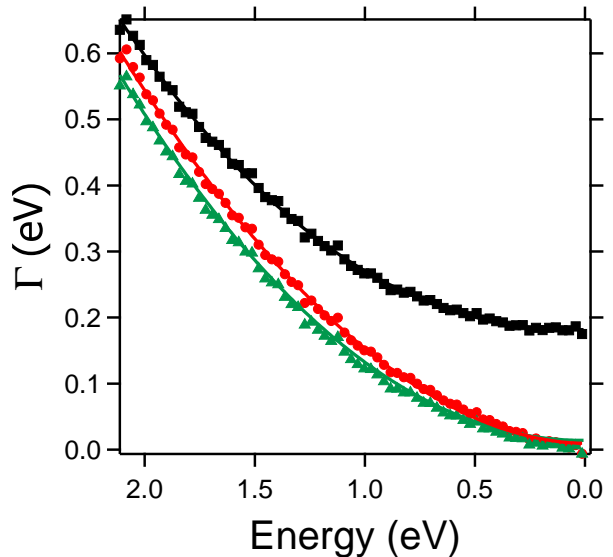


FIG. 6. Presentation of the total scattering rates derived from ARPES (black markers) together with data corrected for energy dependent elastic scattering $\Gamma_h^{\text{el}}(E)$ (green markers) and data corrected for energy dependent “final state“ broadening $\Gamma_h^{\text{fs}}(E)$ (red markers). The solid lines are least squares fit with $\Gamma_h^{\text{fs}}(E) = \alpha E^n$.

Using the experimental broadening at the Fermi level $\Gamma_{\text{exp}} = 0.18$ eV, we derive for the photohole broadening $\Gamma_e = 4.8$ eV. This is a maximal value which may be reduced by finite contributions from elastic scattering. The value, which is expected to be weakly photon energy dependent, is close to $\Gamma_e \approx 3$ eV estimated for a photon energy of 100 eV derived from an analysis of LEED data [28].

Here we remark that the finite energy resolution, although considered in our evaluation, has no influence on our results because it is much smaller ($\Delta E = 0.03$ eV) than the corrections due to elastic scattering and final state effects (0.18 eV). Moreover, we emphasize that an energy dependent matrix element was taken into account in our linewidth analysis [26].

Going back to the case of a broadening which is completely caused by “final state“ effects we derive for the energy dependent initial state broadening

$$\Gamma_h^{\text{fs}}(E) = \Gamma_{\text{exp}}(E)(1 - R(E)) - R(E)\Gamma_e \quad (\text{B8})$$

The data for $\Gamma_h^{\text{fs}}(E)$ corrected for the finite lifetime of the photoelectron are depicted in Fig. 6 by red markers. In this case a least squares fit yields $\alpha = 0.143 \pm 0.002$ and $n = 1.90 \pm 0.02$. The parameters and the corrections are not very different from those using solely elastic scattering contributions.

This comparison shows, that the parameters describing the energy dependent $e - e$ scattering rates Γ_h , presented in the main paper, are nearly independent of the character of the corrections. In the main paper, we present in Fig. 4 the mean value for $\Gamma_h = (\Gamma_h^{\text{el}} + \Gamma_h^{\text{fs}})/2$ and the

corresponding parameters.

-
- [1] T. Dahm, V. Hinkov, S. V. Borisenko, A. A. Kordyuk, V. B. Zabolotnyy, J. Fink, B. Büchner, D. J. Scalapino, W. Hanke, and B. Keimer, *Nature Physics* **5**, 217 (2009).
- [2] A. Damascelli, Z. Hussain, and Z.-X. Shen, *Rev. Mod. Phys.* **75**, 473 (2003).
- [3] J. A. Sobota, Y. He, and Z.-X. Shen, *Rev. Mod. Phys.* **93**, 025006 (2021).
- [4] N. Smith and W. Spicer, *PR* **188**, 593 (1969).
- [5] E. Jensen and E. W. Plummer, *PRL* **55**, 1912 (1985).
- [6] E. W. Plummer, *Physica Scripta* **T17**, 186 (1987).
- [7] I.-W. Lyo and E. W. Plummer, *Phys. Rev. Lett.* **60**, 1558 (1988).
- [8] J. J. Quinn and R. A. Ferrell, *PR* **112**, 812 (1958).
- [9] J. J. Hopfield, *PR* **139**, 419 (1965).
- [10] J. E. Northrup, M. S. Hybertsen, and S. G. Louie, *PRB* **39**, 8198 (1989).
- [11] J. S. Dolado, V. M. Silkin, M. A. Cazalilla, A. Rubio, and P. M. Echenique, *PRB* **64**, 195128 (2001).
- [12] M. Cazzaniga, *PRB* **86**, 035120 (2012).
- [13] J. S. Zhou, M. Gatti, J. J. Kas, J. J. Rehr, and L. Reining, *PRB* **97**, 035137 (2018).
- [14] S. Mandal, K. Haule, K. M. Rabe, and D. Vanderbilt, *Electronic correlation in nearly free electron metals with beyond-dft methods* (2021), arXiv:2101.03262 [cond-mat.str-el].
- [15] T. K. Ng and K. S. Singwi, *PRB* **34**, 7738 (1986).
- [16] F. Nilsson, L. Boehnke, P. Werner, and F. Aryasetiawan, *PRMATERIALS* **1**, 043803 (2017).
- [17] L. Craco and S. Leoni, *PRB* **100**, 115156 (2019).
- [18] X. Zhu and A. W. Overhauser, *PRB* **33**, 925 (1986).
- [19] J. Lischner, T. Bazhiron, A. H. MacDonald, M. L. Cohen, and S. G. Louie, *PRB* **89**, 081108 (2014).
- [20] B. I. Lundqvist, *phys. stat. sol. (b)* **32**, 273 (1969).
- [21] C. M. Varma, P. B. Littlewood, S. Schmitt-Rink, E. Abrahams, and A. E. Ruckenstein, *Phys. Rev. Lett.* **63**, 1996 (1989).
- [22] S. A. Hartnoll and A. P. Mackenzie, *Planckian dissipation in metals* (2021), arXiv:2107.07802 [cond-mat.str-el].
- [23] J. Fink, E. D. L. Rienks, M. Yao, R. Kurlito, J. Bannies, S. Aswartham, I. Morozov, S. Wurmehl, T. Wolf, F. Hardy, C. Meingast, H. S. Jeevan, J. Maiwald, P. Gegenwart, C. Felser, and B. Büchner, *PRB* **103**, 155119 (2021).
- [24] M. Hemmida, N. Winterhalter-Stocker, D. Ehlers, H.-A. K. von Nidda, M. Yao, J. Bannies, E. D. L. Rienks, R. Kurlito, C. Felser, B. Büchner, J. Fink, S. Gorol, T. Förster, S. Arsenijevic, V. Fritsch, and P. Gegenwart, *PRB* **103**, 195112 (2021).
- [25] E. Rienks, M. Arrala, M. Lindroos, F. Roth, W. Tabis, G. Yu, M. Greven, and J. Fink, *Phys. Rev. Lett.* **113**, 137001 (2014).
- [26] R. Kurlito and J. Fink, *Journal of Electron Spectroscopy and Related Phenomena* **253**, 147127 (2021).
- [27] W. Y. Ching and J. Callaway, *PRB* **11**, 1324 (1975).
- [28] J. Pendry, *Photoemission and the electronic properties of surfaces* (Wiley, 1978) p. 87.
- [29] D. E. Eastman, J. A. Knapp, and F. J. Himpsel, *PRL* **41**, 825 (1978).
- [30] P. Thiry, D. Chandesris, J. Lecante, C. Guillot, R. Pinchaux, and Y. Pétroff, *PRL* **43**, 82 (1979).
- [31] J. A. Knapp, F. J. Himpsel, and D. E. Eastman, *Phys. Rev. B* **19**, 4952 (1979).
- [32] T. C. Chiang, J. A. Knapp, M. Aono, and D. E. Eastman, *PRB* **21**, 3513 (1980).
- [33] S. D. Kevan and D. A. Shirley, *PRB* **22**, 542 (1980).
- [34] J. K. Grepstad, B. J. Slagvold, and I. Bartos, *Journal of Physics F: Metal Physics* **12**, 1679 (1982).
- [35] R. A. Bartynski, R. H. Gaylord, T. Gustafsson, and E. W. Plummer, *PRB* **33**, 3644 (1986).
- [36] N. V. Smith, G. K. Wertheim, A. B. Andrews, and C.-T. Chen, *Surface Science* **282**, L359 (1993).
- [37] F. J. Himpsel, *Appl. Opt.* **19**, 3964 (1980).
- [38] J. Fraxedas, J. Trodahl, S. Gopalan, L. Ley, and M. Cardona, *PRB* **41**, 10068 (1990).
- [39] A. B. McLean, C. E. J. Mitchell, and I. G. Hill, *Surface Science* **314**, L925 (1994).
- [40] D. L. Martin, *PR* **124**, 438 (1961).
- [41] T. Valla, A. V. Fedorov, P. D. Johnson, and S. L. Hulbert, *Phys. Rev. Lett.* **83**, 2085 (1999).
- [42] L. Hedin, *PR* **139**, A796 (1965).
- [43] E. V. Chulkov, A. G. Borisov, J. P. Gauyacq, D. Sánchez-Portal, V. M. Silkin, V. P. Zhukov, and P. M. Echenique, *Chem. Rev.* **106**, 4160 (2006).
- [44] A. vom Felde, J. Sprösser-Prou, and J. Fink, *PRB* **40**, 10181 (1989).
- [45] K. Sturm and L. E. Oliveira, *PRB* **40**, 3672 (1989).
- [46] H. Yasuhara, S. Yoshinaga, and M. Higuchi, *PRL* **83**, 3250 (1999).
- [47] M. Elliott and W. R. Datars, *Journal of Physics F: Metal Physics* **12**, 465 (1982).